Author manuscript, published in "Journal of Biological Chemistry 2013;288(34):24910-22"
DOI : 10.1074/jbc.M113.457267

Structural Basis for the Association of MAP6 with Microtubules and its regulation by Calmodulin

Julien Lefèvre[1#]*, Philippe Savarin[1‡], Pierre Gans[2], Loïc Hamon[1], Marie-Jeanne Clément[1], Marie-Odile David[1], Christophe Bosc[3], Annie Andrieux[3] and Patrick A. Curmi[1#]

[1] Institut National de la Santé et de la Recherche Médicale (INSERM), UMR829; Laboratoire Structure-Activité des Biomolécules Normales et Pathologiques ; Université Evry-Val d'Essonne; Evry 91025, France

[2]Laboratoire de Résonance Magnétique Nucléaire, Institut de Biologie Structurale "Jean-Pierre Ebel", 41 rue Jules Horowitz, Grenoble 38027, France

[3]Team Physiopathologie du Cytosquelette, INSERM U836, Institut des Neurosciences, CEA-iRTSV-GPC, Université Joseph Fourier, Site Santé La Tronche, BP170, 38042 Grenoble Cedex 9, France

*Running title: *Microtubule and calmodulin binding on Mn modules of MAP6*

#To whom correspondence should be addressed: Julien Lefèvre, Tel.: 33-1-69-47-01-83; E-mail: julien.lefevre@univ-evry.fr; Patrick Curmi, Tel.: 33-1-69-47-01-87; Fax: 33-1-69-47-02-19; E-mail: pcurmi@univ-evry.fr.

‡present address: Laboratoire CSPBAT (CNRS), UMR 7244, Université Paris 13, Sorbonne Paris Cité, Bobigny 93017, France

Keywords: Calcium; Calmodulin; Cold; MAP6; Microtubules; NMR; STOP; Tubulin

Background: Microtubules are cold-sensitive but some cold-stable microtubules are observed in specific cells due to the presence of MAP6.

Results: Structural data detail how a MAP6 fragment stabilizes microtubules and how calmodulin regulates its activity.

Conclusion: MAP6 may stabilize microtubules by bridging adjacent tubulin heterodimers, an activity sterically hindered by calmodulin.

Significance: This work provides a better understanding of cellular microtubule stabilization and its regulation by calmodulin.

SUMMARY

Microtubules are highly dynamic αβ-tubulin polymers. In vitro and in living cells, microtubules are most often cold and nocodazole sensitive. When present, the MAP6/STOP family of proteins protects microtubules from cold and nocodazole induced depolymerization but the molecular and structure determinants by which these proteins stabilize microtubules remain under debate. We show here that a short protein fragment from MAP6-N which encompasses its Mn1 and Mn2 modules ($MAP6_{90-177}$) recapitulates the function of the full-length MAP6-N protein toward microtubules, i.e. its ability to stabilize microtubules in vitro and in cultured cells in ice-cold condition or in the presence of nocodazole. We further show for the first time, using biochemical assays and NMR spectroscopy, that these effects result from the binding of $MAP6_{90-177}$ to microtubules with a 1:1 $MAP6_{90-177}$:tubulin heterodimer stoichiometry. NMR data demonstrate that the binding of $MAP6_{90-177}$ to microtubules involve its two Mn modules but that a single one is also able to interact with microtubules in a closely similar manner. This suggests that the Mn modules represent each a full microtubule binding domain and that MAP6 proteins may stabilize microtubules by bridging tubulin heterodimers from adjacent protofilaments or within a protofilament. Finally, we demonstrate that Ca^{2+}-calmodulin competes with microtubules for $MAP6_{90-177}$ binding and that the binding mode of $MAP6_{90-177}$ to

inserm-00858655, version 1 - 5 Sep 2013

inserm-00858655, version 1 - 5 Sep 2013

microtubules and Ca^{2+}-calmodulin involves a common stretch of amino acid residues on the $MAP6_{90-177}$ side. This result accounts for the regulation of microtubule stability in cold condition by Ca^{2+}-calmodulin.

In certain cell types such as neurons, fibroblasts or glial cells, a subpopulation of microtubules (MTs) remains stable in depolymerizing conditions such as exposure to the cold or depolymerizing drugs (1-5). Search for cellular factors responsible for this stabilization led to the discovery of a class of microtubule-associated proteins named MAP6 (also called STOP) (6-8). In mammals, MAP6 isoforms are encoded by a single gene (*map6*) and result from mRNA splicing and alternative promoter use (9-11). The physiological role of MAP6 proteins is not yet fully understood but phenotypic and cellular analyses of MAP6 null mice indicated that MAP6 proteins are involved in a number of neuronal functions. MAP6 null mice present defects in synaptic plasticity and neurotransmission associated with severe behavioral disorders (12). Interestingly, these disorders can be alleviated by drugs like neuroleptics suggesting that these mice may represent a valuable animal model for the study of schizophrenia (13). In line with these findings, genetic studies have pointed out a possible link between MAP6 and schizophrenia (14) suggesting that *map6* could be considered as a candidate gene that predispose to schizophrenia and thus be used as a potential biomarker for its early detection (15,16). Besides, MAP6 proteins were also found to be implicated in adult olfactory neurogenesis (17) and MAP6-F (the fibroblastic MAP6 isoform) was proposed to be a temperature sensor that protects MTs from temperature variations in animals during episodes of torpor or hibernation (18).

MAP6-N (the neuronal MAP6 isoform) is the largest MAP6 isoform and is mainly expressed in mature neurons. This 952 residues protein contains several repeated motifs called Mn and Mc modules which are linked to its ability to stabilize MTs (Fig. 1A) (19). The Mn modules allow MAP6 to protect MTs against cold- and nocodazole-induced depolymerization while the Mc modules permit MAP6 to stabilize MTs in cold condition. MAP6-N contains two consecutive Mn modules in its N-terminal part (Mn1 and Mn2) and an additional one isolated in the middle of its sequence (Mn3). The Mc modules are clustered in the central domain as five highly conserved repetitions organized in tandem. Whereas Mn modules are well conserved across species (Fig. 1B), the homology between Mn1, Mn2 and Mn3 is low and they share only a few residues (Fig. 1C). It is worth noting that the number and the organization of Mn and Mc modules can be different among the MAP6 isoforms and this may lead to functional variations toward the propensity of MAP6 proteins to stabilize MTs (8,18,19). In addition, it was shown that the MT stabilization activity of MAP6 proteins is inhibited by calmodulin (CaM) (20,21). Accordingly, peptide arrays revealed that MAP6-N possesses several CaM binding sites, some of which being found in the Mn and Mc modules suggesting that these modules have a dual propensity to interact both with MTs and CaM (19). Very few studies addressed the structural basis of the interaction of MAP6 with MTs and of its interplay with CaM. An NMR study of the interaction between CaM and a peptide model corresponding to the consensus Mc motif showed an unusual interaction mode with a very limited structural impact on the CaM structure (22).

In the present work, we undertook biochemical and structural analyses of the interaction of MAP6-N with MTs and CaM to enlighten the mechanism by which it stabilizes MTs and the mechanisms by which such stabilization is regulated by CaM. As MAP6-N has a high molecular weight, we focused this work on a minimal MAP6-N fragment (residues 90-177, named herein $MAP6_{90-177}$) which recapitulates the MT stabilization and CaM binding properties of MAP6 proteins. We show here that the $MAP6_{90-177}$ fragment, which comprises the Mn1 and Mn2 modules, interacts tightly with MTs and has a powerful MT stabilization activity in vitro and in cultured cells. It also interacts with CaM in a Ca^{2+}-dependent manner. Using a combination of biochemical and NMR experiments, we determined at the residue scale the location of its MT and CaM binding sites and we clearly demonstrated that Ca^{2+}-CaM binding impairs $MAP6_{90-177}$ association with MTs

inserm-00858655, version 1 - 5 Sep 2013

probably because the Ca^{2+}-CaM binding sites substantially overlap the MT binding sites. Furthermore, we examined by NMR the structural impact of $MAP6_{90-177}$ binding on the Ca^{2+}-CaM structure. The results showed dramatic conformational and dynamical changes of Ca^{2+}-CaM affecting its overall structure which led us to propose a binding mode for Ca^{2+}-CaM on the Mn modules of MAP6 proteins.

EXPERIMENTAL PROCEDURES

Transient transfection and immunofluorescence microscopy

The pCMV-FLAG-$MAP6_{90-177}$ plasmid encodes a fusion protein comprising residues 90 to 177 of Rattus norvegicus MAP6-N and was constructed by PCR using a derivative of the pSG5-STOP plasmid as template (8). HeLa cells were grown at 37 °C with 5% CO_2 in Dulbecco's modified Eagle's medium (DMEM) containing 5% fetal bovine serum and 1% penicillin-streptomycin. 5 µg of pCMV-FLAG-$MAP6_{90-177}$ plasmid was mixed with 5 µL of lipofectamine 2000 (Invitrogen, Carlsbad, USA) and then diluted in 200 µL of opti-MEM I. This mix was left for 20 min at 20°C and then added to the HeLa cells culture medium and gently mixed. Cells were returned to the incubator for 4 h at 37°C and the medium was replaced with fresh full medium. 48 h post-transfection, cells were either exposed to cold (on ice for 30 min) or to nocodazole (20 µM for 30 min at 37°C). Cells were then washed twice with PBS and fixed/permeabilized with paraformaldehyde (30 min at 4°C) and cooled methanol (5 min at -20°C). After washing, cells were incubated 1 h at 37 °C with the blocking solution (20 mM Tris-HCl, 150 mM NaCl, 0.1% Triton, 2% BSA, 0.1% NaN_3, pH 7.4). The MT network and $MAP6_{90-177}$ were revealed by immunofluorescence with E7 anti-α-tubulin mouse antibody (1:3000) and anti-FLAG rabbit antibody (1:160) (Sigma-Aldrich, Saint-Louis, USA). Cells were washed twice with PBS and incubated with goat anti-mouse (Alexafluor 488) and anti-rabbit (Alexafluor 594) antibodies. The cells were finally washed with PBS and examined for fluorescence with a Zeiss microscope using a 63x/1.4 numerical aperture objective.

Protein expression and purification

The $MAP6_{90-177}$ fragment was overexpressed in a recombinant form in fusion with an N-terminal polyhistidine tag using the pET-46 Ek/LIC plasmid (Novagen-Merck, Darmstadt, Germany). After transformation with the pET-46 Ek/LIC plasmid, *E. coli* BL21 DE3* cells (Invitrogen, Carlsbad, USA) were grown in LB medium at 37°C with 0.1 mg/mL ampicillin in a 1L flask. For ^{15}N-^{13}C uniform isotopic labeling, transformed bacteria were grown in M9 minimal medium containing 0.6 g/L 95% $^{15}NH_4Cl$ and 2.2 g/L 95% ^{13}C-glucose (Cortecnet, Paris, France) as the sole nitrogen and carbon sources respectively. In all cases, overexpression was induced at $OD_{600\ nm}$ = 0.7 with 1 mM IPTG for 2 h. Bacteria were pelleted by low speed centrifugation (3,200 x g, 10 min) and then resuspended in 10 mL of buffer A (20 mM Tris-HCl, 100 mM NaCl, 1 mM DTT, pH 7.6). After lysis by sonication, the lysate was heated for 25 min at 95°C and then ultracentrifuged at 4°C (100,000 x g, 1 h). The clarified cell lysate was then loaded on a Ni-NTA column (Qiagen, Hilden, Germany) equilibrated with buffer A supplemented with 10 mM imidazole. The proteins were eluted with buffer B (20 mM Tris-HCl, 100 mM NaCl, 1 mM DTT, 300 mM imidazole, pH 7.6). Fractions containing the $MAP6_{90-177}$ were combined and concentrated by ultrafiltration (Amicon 3 kDa cutoff, Millipore) at 4°C to 0.5 mL and diluted into 4.5 mL buffer C (50 mM MES-KOH, 150 mM NaCl, 1 mM DTT, pH 6.9). The procedure of concentration/dilution was repeated three times with buffer C to eliminate imidazole. Final concentration of $MAP6_{90-177}$ was determined by amino acid analysis. The result was used to determine the extinction coefficient of $MAP6_{90-177}$ (ε_{280nm} = 2.3 x 10^4 $M^{-1}.cm^{-1}$). The final yield was about 1 mg/L of pure protein. The $MAP6_{90-142}$ fragment (residues 90-142 of Rattus norvegicus MAP6-N) was obtained using the same protocol (ε_{280nm} = 9.2 x 10^3 $M^{-1}.cm^{-1}$) with a final yield of 3 mg/L of pure peptide. All the purification steps were performed in the presence of protease inhibitors cocktails (Roche, Basel, Switzerland and Halt, Thermo Scientific, Brebières, France) complemented with 0.1 mg/mL TPCK and TLCK.

CaM from bovine brain was purchased as a lyophilized powder (Sigma-Aldrich). ^{15}N-^{13}C-labeled CaM was expressed and purified according to Bouvier et al. (22).

inserm-00858655, version 1 - 5 Sep 2013

Tubulin was purified from sheep brain using the method of Castoldi and Popov (23) and stored in liquid nitrogen. Before use, an additional cycle of polymerization/depolymerization was performed and tubulin was resuspended in 50 mM MES-KOH, 4.1 M glycerol, 1 mM $MgCl_2$, 0.5 mM EGTA, pH 6.9. Tubulin concentration was determined by spectrophotometry using an extinction coefficient $\varepsilon_{278nm} = 1.2 \times 10^5\ M^{-1}.cm^{-1}$.

Binding of MAP6-N fragments to MTs and MT stabilization Assays

For MT co-sedimentation assays, tubulin was polymerized for 30 min at 37°C in 40 mM MES-KOH, 4 mM $MgCl_2$, 1 mM DTT, 1 mM GTP, 2.7 M glycerol, pH 6.9 (buffer P) with stoichiometric amounts of taxol. 0, 5, 15 or 25 µM of taxol-stabilized MTs were then incubated with 20 µM $MAP6_{90\text{-}177}$ for 15 min at 20°C. MT pellets were collected by centrifugation (25,000 x g, 40 min at 20°C). To obtain MT binding saturation data, co-sedimentation experiments were performed using a range of concentrations of $MAP6_{90\text{-}177}$ (0-50 µM) and a fixed amount of taxol-stabilized MTs (10 µM). After 10 min incubation at 20°C, MT-bound $MAP6_{90\text{-}177}$ was obtained by centrifugation (25,000 x g, 40 min at 20°C) and estimated by SDS-PAGE using an Odyssey Imaging System (LI-COR Biosciences, Lincoln, NE, USA). The molar binding stoichiometry and dissociation constant (K_d) were determined graphically. The same procedure was used for co-sedimentation assays in the presence of Ca^{2+}-CaM (35 µM taxol-stabilized MTs, 10 µM $MAP6_{90\text{-}177}$, 0.2 mM $CaCl_2$, 0, 40 and 80 µM CaM, incubation for 5 min at 20°C). For MT cold stability assays, 25 µM tubulin was polymerized in buffer P for 30 min at 37°C without (control) or with 20 µM $MAP6_{90\text{-}177}$. After incubation on ice for 10 min, MT pellets and supernatants were separated by centrifugation (25,000 x g, 40 min, 4°C). To evaluate the influence of Ca^{2+}-CaM on the ability of $MAP6_{90\text{-}177}$ to stabilize MTs in cold condition, we used the same procedure in the presence of CaM (35 µM MT, 0.5 mM spermine and 50 µM $CaCl_2$ were first incubated for 10 min at 37°C with 25 µM $MAP6_{90\text{-}177}$ alone or in the presence of 100 µM CaM, followed by an incubation for 10 min on ice). The kinetics of MT polymerization were monitored turbidimetrically at 370 nm (1 cm path) in an Ultrospec 3000 spectrophotometer (GE Healthcare, Fairfield, USA) equipped with a temperature controller. 35 µM tubulin was polymerized with 0, 0.35, 3.5 and 35 µM $MAP6_{90\text{-}177}$ in buffer P at 37°C. At the steady state, MT destabilization was induced by a cold shock (4°C) for 2 min. To verify the integrity of the tubulin after the cold treatment, the temperature was then set again at 37°C. The presence of MTs after the cold shock was examined by atomic force microscopy (AFM) on 10 µL aliquots containing 35 µM $MAP6_{90\text{-}177}$ and sampled at t = 30 min. The samples were deposited on freshly cleaved mica and dried for AFM imaging as described previously (24). All AFM experiments were performed in intermittent mode with a multimode AFM instrument (Digital Instruments, Veeco, Santa Barbara, USA) operating with a Nanoscope IIIa controller (Digital Instruments). Images were collected at a scan frequency of 1.5 Hz and a resolution of 512 x 512 pixels.

Immobilized CaM-binding assay

CaM-agarose beads (Sigma-Aldrich) were equilibrated in 50 mM MES-KOH, 1 mM $CaCl_2$, pH 6.9 and incubated with pure $MAP6_{90\text{-}177}$ for 30 min at 20°C. Beads were then washed with the same buffer. Flow-through, washes and CaM-beads fractions were analyzed on SDS-PAGE and the proteins revealed by Coomassie blue staining. The Ca^{2+}-dependence of this interaction was tested with calcium-free buffer supplemented with 5 mM EGTA.

Isothermal titration calorimetry (ITC)

ITC measurements were performed at 25°C using an ITC_{200} calorimeter (GE Healthcare, Fairfield, USA). Samples were thoroughly degassed before each titration. Titration and sample solutions were prepared in 20 mM MES-KOH, 50 mM NaCl, 1 mM DTT either with 1 mM $CaCl_2$ or 5 mM EGTA, pH 6.9. Titrations were carried out by injecting 25 consecutive aliquots (1.5 µL) of 200 µM $MAP6_{90\text{-}177}$ into the ITC cell (0.2 mL) containing 25 µM CaM. A background titration consisting of the identical titration solution but containing only the buffer in the cell was subtracted from each titration to quantify heat produced by sample dilution. The value obtained was subtracted from the heat of reaction to give the effective heat of binding. The resulting titration data were analyzed using the ORIGIN software (MicroCal Inc., Northampton, USA). The molar binding stoichiometry, binding

inserm-00858655, version 1 - 5 Sep 2013

constant ($K_a = 1/K_d$) and binding enthalpy (ΔH) were determined by fitting the binding isotherm to a model with one set of sites. For the fit, no constraint in stoichiometry, K_a and ΔH was introduced. Changes in free energy (ΔG) and in entropy ($T\Delta S$) were calculated from $\Delta G = -RT \ln K_a = \Delta H - T\Delta S$, where R is the gas constant and T the temperature in Kelvin.

NMR experiments

$MAP6_{90-177}$ and $MAP6_{90-142}$ NMR spectra were acquired at 20°C on a Bruker Avance 600 NMR spectrometer using a cryoprobe. All experiments were performed in 50 mM MES-KOH, 150 mM NaCl, 1mM DTT, pH 6.9 on 60 µL samples using the MATCH^{TM} system (Cortecnet, Paris, France). Three-dimensional NOESY- and TOCSY-^{1}H-^{15}N HSQC and HNCO, HNCA, HN(CA)CO, CBCA(CO)NH experiments were performed for backbone assignments on a 500 µM ^{15}N- or ^{15}N-^{13}C-labeled $MAP6_{90-177}$ sample (25). All spectra were processed with Topspin 2.0 and NMRView (26).

^{1}H-^{15}N HSQC experiments were used to characterize the interaction of $MAP6_{90-177}$ and $MAP6_{90-142}$ with tubulin, taxol-stabilized MTs, apoCaM, Ca^{2+}-CaM and BSA (negative control). Titration series were performed using ^{15}N-labeled $MAP6_{90-177}$ or $MAP6_{90-142}$ samples dissolved in 50 mM MES-KOH, 150 mM NaCl, 1 mM DTT, pH 6.9 at 6°C for tubulin and taxol-stabilized MTs and 20°C for CaM. Spectra were recorded using 128 x 2048 complex data points in F1 and F2 dimensions with 16 scans per increment. The spectral widths were 1202 and 1500 Hz in the ^{15}N and ^{1}H dimensions respectively.

A Ca^{2+}-loaded uniformly ^{15}N-^{13}C-labeled CaM sample was prepared at 60 µM in 18 mM Tris-HCl, pH 7.8 and 10% D_2O and studied in Shigemi tube (Shigemi Inc., Allison Park, PA). The formation of the $MAP6_{90-177}$:Ca^{2+}-CaM complex was examined on samples by direct addition of different aliquots of a concentrated solution of unlabeled $MAP6_{90-177}$ (from a 0.6 mM stock solution) to the ^{15}N-^{13}C-labeled Ca^{2+}-CaM NMR sample to reach 1.5:1 $MAP6_{90-177}$:Ca^{2+}-CaM stoichiometry. NMR spectra were acquired at 27 °C on an Agilent VNMRS 800 MHz spectrometer using a cryoprobe. BEST-TROSY experiment was used as it provides resolution without losing sensitivity compared to ^{1}H-^{15}N HSQC (27). 128 x 930 complex points in the F1 and F2 dimensions were acquired for an experimental time of about 3 h. All data were processed using the NMRPipe software (28). Figures are represented with the VMD software (29).

RESULTS

$MAP6_{90-177}$ induces MT resistance to cold and nocodazole in HeLa cultured cells. As a prerequisite to biochemical and structural investigation, we verified the functionality of the $MAP6_{90-177}$ fragment toward MT stabilization in cultured HeLa cells. HeLa cells are well suited for this kind of experiments because they do not endogenously express MAP6 proteins and are devoid of cold-stable and drug-resistant MTs (30). HeLa cells were transfected with the pCMV-FLAG-$MAP6_{90-177}$ vector and examined for MT resistance to the cold and nocodazole. Results show that all the transfected cells exhibit a clearly visible MT network whereas non-transfected cells show a diffuse labeling. Additionally, analysis of the distribution of $MAP6_{90-177}$ in transfected cells shows that it colocalizes with the MT network suggesting that MT stabilization by $MAP6_{90-177}$ is direct (Fig. 2). As $MAP6_{90-177}$ thus binds to and stabilizes MTs in a cellular context, the investigation of its biochemical and structural properties appears of interest for the characterization of the full length MAP6 proteins.

$MAP6_{90-177}$ binds to MTs and induces MT resistance to cold in vitro. As a second step, to distinguish between a direct and indirect binding through putative protein partners, we analyzed the association of $MAP6_{90-177}$ with MTs in vitro using co-sedimentation experiments with taxol-stabilized MTs. In the absence of MT, $MAP6_{90-177}$ was not detectable in the pellet demonstrating that $MAP6_{90-177}$ is soluble in these conditions. When $MAP6_{90-177}$ was incubated with increasing amounts of MTs, a concentration-dependent $MAP6_{90-177}$ binding to MTs was observed (Fig. 3A). This result shows that $MAP6_{90-177}$ binds directly to MTs. In addition, we found that shearing MTs, which increases the number of MT ends, did not significantly affect $MAP6_{90-177}$ binding to MTs (data not shown). To further characterize the $MAP6_{90-177}$:MT interaction, $MAP6_{90-177}$ at different concentrations was then

inserm-00858655, version 1 - 5 Sep 2013

incubated with a fixed amount of taxol-stabilized MTs (Fig. 3B). MTs were then pelleted and the $MAP6_{90-177}$ content was analyzed by SDS-PAGE and quantified. The results show that the binding of $MAP6_{90-177}$ to MTs is saturable with an estimated K_d of 6 μM and a 1:1 $MAP6_{90-177}$:tubulin heterodimer stoichiometry.

We then assessed the ability of the $MAP6_{90-177}$ fragment to stabilize MTs against cold. After polymerization of tubulin into MTs at 37°C, MTs were exposed to cold (ice, 10 min) in the absence or presence of $MAP6_{90-177}$. SDS-PAGE analysis shows that the amount of MTs in the pellet increases dramatically in the presence of $MAP6_{90-177}$ after cold treatment (Fig. 3C). Similar results were observed whether the $MAP6_{90-177}$ fragment was mixed to tubulin before polymerization or added to assembled MTs. To confirm that the $MAP6_{90-177}$ fragment truly protected MTs from cold depolymerization, we examined the dynamics of MT assembly by turbidimetry at 370 nm (Fig. 3D). Results show that the kinetics of tubulin polymerization are very similar in the absence or presence of different concentrations of $MAP6_{90-177}$ demonstrating that $MAP6_{90-177}$ has no impact on the nucleation and elongation steps. In addition, the steady state turbidity value was also similar in both cases suggesting that no particular supra-assembly of MTs such as bundles were formed in the presence of $MAP6_{90-177}$. The cold shock was performed at steady state. In the control condition, it induced a clear MT depolymerization. The effect of this cold shock diminished dramatically in the presence of $MAP6_{90-177}$, and a total protection was observed when the $MAP6_{90-177}$:tubulin heterodimer ratio reached a value of about 1:1. To ascertain that the macromolecular objects diffusing light during the cold shock in the presence of $MAP6_{90-177}$ are really MTs, we performed AFM imaging which shows filamentous structures with length and width in good agreement with MT dimensions (31) (Fig. 3E).

Quantification of the $MAP6_{90-177}$:CaM interaction. It was previously demonstrated that MAP6-N binds to CaM (8) and that Mn modules are in part implicated in this interaction (19). To further investigate such interaction, we examined the binding of $MAP6_{90-177}$ to CaM immobilized on beads (Fig. 4A). The results show that $MAP6_{90-177}$ is able to bind to CaM but only in the presence of $CaCl_2$. Indeed, when the binding experiment was realized with 5 mM EGTA instead of $CaCl_2$, no binding was observed demonstrating that calcium is necessary for this interaction.

We next carried out ITC experiments to quantify the $MAP6_{90-177}$:CaM interaction. Figure 4B displays the binding isotherm of $MAP6_{90-177}$ titration into the Ca^{2+}-CaM solution. The best fit of the integrated isotherm indicated that one $MAP6_{90-177}$ binds to two Ca^{2+}-CaM molecules with a K_d value of 0.4 μM (Fig. 4C). The same ITC experiment carried out with EGTA in place of $CaCl_2$ showed no detectable interaction.

Identification of $MAP6_{90-177}$ residues implicated in the interaction with MTs and Ca^{2+}-CaM. Large amounts of pure and soluble $MAP6_{90-177}$ could be obtained from recombinant expression in *E. coli* which allowed NMR study of $MAP6_{90-177}$ interactions with its partners at the residue scale. ^{1}H-^{15}N HSQC spectrum of $MAP6_{90-177}$ in aqueous buffer shows well resolved resonances with a weak dispersion of correlation peaks (less than 1 ppm and about 20 ppm on the ^{1}H and ^{15}N dimensions respectively) suggesting that under these conditions the $MAP6_{90-177}$ does not fold into any defined tertiary structure (Fig. 5A). NMR assignment of the backbone resonances of $MAP6_{90-177}$ was achieved (Supp. files, Table 1). Analysis of the chemical shifts deviations from random coil values of ^{13}CO and $^{13}C\alpha$ (32) also indicated that $MAP6_{90-177}$ does not contain significant secondary structure (Fig. 5B). In agreement with this, we observed that during the course of overexpression and purification, the $MAP6_{90-177}$ fragment exhibited a high sensitivity to protease degradation together with a high thermostability, properties that are frequently observed for intrinsically unstructured proteins.

In order to identify $MAP6_{90-177}$ residues that mediate MT and Ca^{2+}-CaM interaction, ^{1}H-^{15}N HSQC spectra of free ^{15}N- $MAP6_{90-177}$ and bound to unlabeled tubulin, MTs and Ca^{2+}-CaM were recorded (Fig. 6A). Because of the large size of these complexes, many ^{1}H-^{15}N cross-peaks of residues implicated in the interaction underwent line broadening and disappeared which helped us to point them out. Experiments carried out either with tubulin or MTs gave identical results whereas control experiments performed with BSA showed no modification. A peak by peak analysis using assignment of $MAP6_{90-177}$ allowed us to define two MT binding sites delimited by

inserm-00858655, version 1 - 5 Sep 2013

residues 121-138 and 150-175 (Fig. 6A). As the C-terminal tail of tubulin is a major binding site for many MT partners, we tested whether this part of tubulin is implicated in the $MAP6_{90-177}$:MT interaction. Co-sedimentation assays were carried out in the presence of an excess of a recombinant tubulin fragment corresponding to the C-terminal tail of α-tubulin (αTub410C) (33) (Supp. files, Fig. S1). Results show that this αTub410C fragment did not compete with MTs for $MAP6_{90-177}$ binding. This result was confirmed by NMR which showed that the ^{1}H-^{15}N HSQC spectrum of ^{15}N-$MAP6_{90-177}$ remained identical in the absence or in the presence of an excess of unlabeled αTub410C (data not shown).

We then attempted to locate the Ca^{2+}-CaM binding site on $MAP6_{90-177}$ using similar ^{1}H-^{15}N HSQC mapping experiments (Fig. 6A). As seen for MTs, Ca^{2+}-CaM binding to ^{15}N-$MAP6_{90-177}$ induced line broadening due to the large size of the complex. The mapping of the Ca^{2+}-CaM binding site points out two regions delimited by residues 121-137 and 151-176 which are very similar to those that participate to the binding of MTs. Surprisingly, this suggests a common binding mode for MTs and Ca^{2+}-CaM. Finally, the binding of $MAP6_{90-177}$ to Ca^{2+}-CaM could be reversed with EGTA confirming again the Ca^{2+}-dependence of the $MAP6_{90-177}$:CaM interaction (data not shown).

We then examined by competition experiments whether Ca^{2+}-CaM could impair $MAP6_{90-177}$ binding to MTs (Fig. 6B). Taxol-stabilized MTs were incubated in the presence of a fixed amount of $MAP6_{90-177}$ and increasing concentrations of Ca^{2+}-CaM. Free and MT-bound $MAP6_{90-177}$ were then separated by centrifugation and analyzed by SDS-PAGE and Coomassie blue staining. Results indicate a progressive displacement of $MAP6_{90-177}$ from pellet to supernatant as the concentration of Ca^{2+}-CaM increases. Hence, it appears that MTs and Ca^{2+}-CaM bind to $MAP6_{90-177}$ in a mutually exclusive manner. This competition was confirmed in functional assays in which the protective effect of $MAP6_{90-177}$ for MT cold depolymerization was tested in the presence of Ca^{2+}-CaM (Fig. 6C). In this experiment, Ca^{2+} was required to obtain the holo-form of CaM. However, due to the destabilizing effect of Ca^{2+} on MTs, experiments were performed in the presence of excess of spermine which acts as a Ca^{2+} competitive inhibitor for MT binding (33). Polymerized MTs were incubated on ice alone (control, the two left lanes) or with $MAP6_{90-177}$ (the two middle lanes) or with $MAP6_{90-177}$ and Ca^{2+}-CaM (the two right lanes). Results show clearly that $MAP6_{90-177}$ no longer protects MTs in the presence of Ca^{2+}-CaM.

Binding of $MAP6_{90-177}$ to Ca^{2+}-CaM induces large conformational changes of the Ca^{2+}-CaM structure. In order to study the structural impact of $MAP6_{90-177}$ binding on the Ca^{2+}-CaM structure, we carried out NMR experiments with purified and ^{15}N-^{13}C-labeled Ca^{2+}-CaM. BEST-TROSY spectra of ^{15}N-^{13}C-Ca^{2+}-CaM in the absence and presence of unlabeled $MAP6_{90-177}$ were recorded (Fig. 7A). The addition of $MAP6_{90-177}$ to Ca^{2+}-CaM resulted in very large changes of the spectrum profile of Ca^{2+}-CaM with modifications of the peaks number and of the chemical shifts distribution. Residues affected by this interaction are reported on the CaM sequence and on a crystallographic structure of Ca^{2+}-CaM (34) (Fig. 7B and 7C). Results show that the perturbations are found mostly in the N-terminal domain and in the central α helix of Ca^{2+}-CaM. Indeed, NMR mapping points out a first stretches in the N-terminal domain (residues 13-39) and a second long stretches comprising the end of the N-terminal domain and more than half the central α helix (residues 49-80). The C-terminal domain is affected but in a lesser extent. Together, these observations indicate that the binding of $MAP6_{90-177}$ induces wide-range conformational and dynamical changes in the Ca^{2+}-CaM structure implicating mostly its N-terminal domain and the central α-helix.

MTs and Ca^{2+}-CaM compete for the same binding site on the Mn1 module. We finally examined the possibility that a single Mn module could interact with MTs and Ca^{2+}-CaM. To that end, we overexpressed and purified a 53 amino acid residues fragment encompassing the N-terminal part and the Mn1 module of $MAP6_{90-177}$ (MAP6-N residues 90-142, named herein $MAP6_{90-142}$). We observed that the ^{1}H-^{15}N HSQC spectrum of $MAP6_{90-142}$ superimposes very well with that of the $MAP6_{90-177}$ fragment which strongly facilitated its assignment. When the $MAP6_{90-142}$ fragment was studied in the presence of tubulin or MTs, we observed on its ^{1}H-^{15}N HSQC spectrum (Fig. 8A) line broadening

inserm-00858655, version 1 - 5 Sep 2013

responsible for the disappearance of some peaks corresponding to the stretch of residues 121-138 with the exception of C135 (Fig. 8B). Interestingly, the ^{1}H-^{15}N HSQC spectrum of $MAP6_{90-142}$ acquired in the presence of Ca^{2+}-CaM (Fig. 8A) gave very close results with line broadening and disappearance of peaks corresponding to residue V118 and of the stretch 121-138 except Q129 and S134 (Fig. 8B). Hence, these results show that the Mn1 module, when considered isolated from the other Mn modules, is able to bind to both MTs and Ca^{2+}-CaM in a similar manner.

DISCUSSION

$MAP6_{90-177}$ binds and stabilizes MTs - The aim of this work was to better understand the molecular mechanisms underlying the stabilization of MTs by MAP6 and its regulation by CaM using biochemical and structural investigations. To that end, we took advantage of a MAP6-N fragment encompassing its Mn1 and Mn2 modules which recapitulates the functional properties of the full length protein. As a first step, we studied the interaction between $MAP6_{90-177}$ and MTs. Using co-sedimentation assays, we found that $MAP6_{90-177}$ interacts with MTs with an apparent K_d value of about 6 μM and a 1:1 $MAP6_{90-177}$:tubulin heterodimer stoichiometry (Fig. 3B). To the best of our knowledge, this is the first report on a K_d value regarding the interaction of Mn modules with MTs. Delphin et al. reported a K_d value of about 70 nM for the interaction between the Mc domain of MAP6-F and MTs (18). The lower apparent affinity observed here for $MAP6_{90-177}$ may be related to the fact that this fragment contains only two Mn modules whereas the Mc domain contains five Mc modules. This suggests that the binding of MAP6 to MTs may be cooperative. Co-sedimentation assays (Supp. files, Fig. S1) and NMR experiments (data not shown) using a α–tubulin C-terminal fragment (αTub410C, residues 410–451 from α1a-tubulin (33)) indicated that this part of tubulin is not sufficient for the interaction with $MAP6_{90-177}$. This agrees with previous report showing that, unlike other MAPs, MAP6 can bind significantly to any tubulin isoform whatever its degree of C-terminal modification by polyglutamylation (35).

We observed that the stabilization of MTs against cold and nocodazole by $MAP6_{90-177}$ does not induce MT aggregates nor bundles in contrast to what was observed with full length MAP6-N by immunofluorescence microscopy (7). In this later case, the formation of MT bundles may be due either to the presence of multiple Mn and Mc repeats or to a possible multimerization of the protein via stretches of amino acid residues that are located outside the $MAP6_{90-177}$ region. We next mapped the $MAP6_{90-177}$ interaction with MTs to two $MAP6_{90-177}$ binding sites defined by residues 121-138 and 150-175 which correlate strongly with Mn1 and Mn2 modules respectively (19). Interestingly, NMR data show that a single Mn module ($MAP6_{90-142}$) can still interact with MTs suggesting that each Mn module in MAP6 may serve as anchor point for MT binding. Accordingly, each Mn repeat may recognize a conserved binding motif located on α- and β-tubulin. From a structural point of view, MT stabilization by $MAP6_{90-177}$ is thus likely to occur through the reinforcement of the longitudinal contacts between tubulin heterodimers within a protofilament as seen for Tau (36) or lateral contacts between adjacent tubulin heterodimers preventing protofilaments separation like the stabilization mode of doublecortin (37). In addition, we cannot exclude that $MAP6_{90-177}$ may also stabilize MTs by preventing cold- or nocodazole-induced conformational changes in tubulin by a more complex mechanism.

Association of $MAP6_{90-177}$ with MTs is regulated by Ca^{2+}-CaM - Biochemical and ITC experiments showed that $MAP6_{90-177}$ binds to CaM in a Ca^{2+}-dependent manner with a K_d value of 0.4 μM and a 1:2 $MAP6_{90-177}$:Ca^{2+}-CaM stoichiometry (Fig. 4). This K_d value lies in the range of that previously reported for MAP6-F:Ca^{2+}-CaM (K_d ~ 1.7 and 8.1 μM) (19) and Mc:Ca^{2+}-CaM (K_d ~ 1.5 and 3.9 μM) interactions (22,38). Such an affinity is compatible with a physiological interaction of Ca^{2+}-CaM with MAP6 for instance after a transient rise in cytoplasmic [Ca^{2+}]. Investigation of $MAP6_{90-177}$:Ca^{2+}-CaM interaction by NMR pointed out two $MAP6_{90-177}$ regions (121-137 and 151-176) which are nearly identical to the $MAP6_{90-177}$:MTs binding sites. This suggests that Ca^{2+}-CaM may compete with MTs for $MAP6_{90-177}$ binding. In agreement with this hypothesis, we demonstrated for the first time using co-sedimentation assays that Ca^{2+}-CaM is responsible for a stoichiometric inhibition of $MAP6_{90-177}$ binding to MTs

inserm-00858655, version 1 - 5 Sep 2013

resulting in a loss of MT stabilization. Altogether, these observations suggest that the regulation of MAP6 binding to MTs by Ca^{2+}-CaM is a dynamic process rapidly modulated by the Ca^{2+}-charge state of CaM. A similar mechanism was proposed for Tau in the flip-flop model (39). Finally, this part of MAP6-N also comprises S139 which can be phosphorylated by the Ca^{2+}-Calmodulin-dependent protein kinase II (CaMKII) which triggers the translocation of MAP6 from MTs to actin (40). Interestingly, this kind of regulation has already been observed for the microtubule-associated protein p35 which is also regulated by site-specific phosphorylations and Ca^{2+}-CaM with MT overlapping binding sites (41). Similar mechanisms of CaM regulation were again suggested for Tau (42-44).

Impact of $MAP6_{90-177}$ on Ca^{2+}-CaM structure, implication for the binding mode - Previous NMR, infrared spectroscopy and differential scanning calorimetry investigations on the interaction of Ca^{2+}-CaM with a model peptide corresponding to a single Mc motif revealed an unusual binding mode. Indeed, these studies showed that the Mc peptide interacts with the C-terminal domain of CaM leaving it in an extended conformation with no significant structural change (22)(38). The present data provide strong evidences that the binding mode of $MAP6_{90-177}$ to Ca^{2+}-CaM is distinct from that previously observed with Mc modules. However, the present NMR data show that the binding of $MAP6_{90-177}$ to Ca^{2+}-CaM produces large structural and dynamical changes in Ca^{2+}-CaM. Interestingly, sequence analysis of the two sites of $MAP6_{90-177}$ that interact with Ca^{2+}-CaM, suggests that they belong to the 1-5-10 class of canonical CaM-binding motifs found in several CaM-regulated proteins such as CaMKII and Synapsin I (45,46) (Fig. 9). This class refers to a group of Ca^{2+}-CaM partners whose key hydrophobic bulky residues are spaced by eight residues with an additional anchoring residue in the middle. Upon binding, both Ca^{2+}-CaM and the target peptide motif undergo large conformational rearrangements. The canonical CaM-binding motif adopts a α-helical conformation and the two domains of CaM wraps around it, enclosing it in a hydrophobic channel within the globular core. The data obtained here on $MAP6_{90-177}$:Ca^{2+}-CaM interaction argue for a similar binding mode: i) Ca^{2+} is required for $MAP6_{90-177}$ binding, a fact that is systematically observed with this type of binding mode; ii) large structural modifications of the Ca^{2+}-CaM structure are observed affecting its two domains and its central flexible helix and iii) secondary structure prediction of $MAP6_{90-177}$ show that residues 117-125 and 148-158 may fold into α–helices. These stretches overlap the 1-5-10 motifs of $MAP6_{90-177}$ and it is possible that they locally fold when in complex with Ca^{2+}-CaM. It is worthy to note that neither the Mc modules nor the Mn3 module of MAP6 (which bind to Ca^{2+}-CaM) contain such 1-5-10 motif. This may explain previous reports showing an unusual binding mode for these CaM-binding sites (22) (Pierre Gans, personal communication). Interestingly, some 1-5-10 motifs were shown to be implicated both in Ca^{2+}-CaM and actin binding (47-49) and MAP6-N was shown to interact with actin (40). It would be of interest to probe whether this region is implicated in MAP6-N association with actin and whether Ca^{2+}-CaM binding to this region may regulate such process.

In conclusion we report here for the first time structure and functional information on a short region from MAP6 that recapitulates its ability to bind and stabilize MTs upon exposure to cold or nocodazole. The binding of this region to MTs appears modulated by a competitive interaction with Ca^{2+}-CaM which further documents the complex regulation of MT assembly by MAP6.

inserm-00858655, version 1 - 5 Sep 2013

REFERENCES

1. **Webb, B. C., and Wilson, L. (1980) Cold-stable microtubules from brain. *Biochemistry* 19, 1993-2001**
2. **Baas, P. W., and Heidemann, S. R. (1986) Microtubule reassembly from nucleating fragments during the regrowth of amputated neurites. *J Cell Biol* 103, 917-927**
3. **Baas, P. W., Slaughter, T., Brown, A., and Black, M. M. (1991) Microtubule dynamics in axons and dendrites. *J Neurosci Res* 30, 134-153**
4. **Guillaud, L., Bosc, C., Fourest-Lieuvin, A., Denarier, E., Pirollet, F., Lafanechere, L., and Job, D. (1998) STOP proteins are responsible for the high degree of microtubule stabilization observed in neuronal cells. *J Cell Biol* 142, 167-179**
5. **Galiano, M. R., Bosc, C., Schweitzer, A., Andrieux, A., Job, D., and Hallak, M. E. (2004) Astrocytes and oligodendrocytes express different STOP protein isoforms. *J Neurosci Res* 78, 329-337**
6. **Margolis, R. L., Rauch, C. T., and Job, D. (1986) Purification and assay of a 145-kDa protein (STOP145) with microtubule-stabilizing and motility behavior. *Proc Natl Acad Sci U S A* 83, 639-643**
7. **Margolis, R. L., Rauch, C. T., Pirollet, F., and Job, D. (1990) Specific association of STOP protein with microtubules in vitro and with stable microtubules in mitotic spindles of cultured cells. *EMBO J* 9, 4095-4102**
8. **Bosc, C., Cronk, J. D., Pirollet, F., Watterson, D. M., Haiech, J., Job, D., and Margolis, R. L. (1996) Cloning, expression, and properties of the microtubule-stabilizing protein STOP. *Proc Natl Acad Sci U S A* 93, 2125-2130**
9. **Denarier, E., Fourest-Lieuvin, A., Bosc, C., Pirollet, F., Chapel, A., Margolis, R. L., and Job, D. (1998) Nonneuronal isoforms of STOP protein are responsible for microtubule cold stability in mammalian fibroblasts. *Proc Natl Acad Sci U S A* 95, 6055-6060**
10. **Denarier, E., Aguezzoul, M., Jolly, C., Vourc'h, C., Roure, A., Andrieux, A., Bosc, C., and Job, D. (1998) Genomic structure and chromosomal mapping of the mouse STOP gene (Mtap6). *Biochem Biophys Res Commun* 243, 791-796**
11. **Aguezzoul, M., Andrieux, A., and Denarier, E. (2003) Overlap of promoter and coding sequences in the mouse STOP gene (Mtap6). *Genomics* 81, 623-627**
12. **Andrieux, A., Salin, P. A., Vernet, M., Kujala, P., Baratier, J., Gory-Faure, S., Bosc, C., Pointu, H., Proietto, D., Schweitzer, A., Denarier, E., Klumperman, J., and Job, D. (2002) The suppression of brain cold-stable microtubules in mice induces synaptic defects associated with neuroleptic-sensitive behavioral disorders. *Genes Dev* 16, 2350-2364**
13. **Delotterie, D., Ruiz, G., Brocard, J., Schweitzer, A., Roucard, C., Roche, Y., Suaud-Chagny, M. F., Bressand, K., and Andrieux, A. (2010) Chronic administration of atypical antipsychotics improves behavioral and synaptic defects of STOP null mice. *Psychopharmacology (Berl)* 208, 131-141**
14. **Shimizu, H., Iwayama, Y., Yamada, K., Toyota, T., Minabe, Y., Nakamura, K., Nakajima, M., Hattori, E., Mori, N., Osumi, N., and Yoshikawa, T. (2006) Genetic and expression analyses of the STOP (MAP6) gene in schizophrenia. *Schizophr Res* 84, 244-252**
15. **Choi, K. H., Zepp, M. E., Higgs, B. W., Weickert, C. S., and Webster, M. J. (2009) Expression profiles of schizophrenia susceptibility genes during human prefrontal cortical development. *J Psychiatry Neurosci* 34, 450-458**
16. **Martins-De-Souza, D., Dias-Neto, E., Schmitt, A., Falkai, P., Gormanns, P., Maccarrone, G., Turck, C. W., and Gattaz, W. F. (2010) Proteome analysis of schizophrenia brain tissue. *World J Biol Psychiatry* 11, 110-120**
17. **Benardais, K., Kasem, B., Couegnas, A., Samama, B., Fernandez, S., Schaeffer, C., Antal, M. C., Job, D., Schweitzer, A., Andrieux, A., Giersch, A., Nehlig, A., and Boehm, N. (2010) Loss of STOP protein impairs peripheral olfactory neurogenesis. *PLoS One* 5, e12753**

18. **Delphin, C., Bouvier, D., Seggio, M., Couriol, E., Saoudi, Y., Denarier, E., Bosc, C., Valiron, O., Bisbal, M., Arnal, I., and Andrieux, A. (2012) MAP6-F Is a Temperature Sensor That Directly Binds to and Protects Microtubules from Cold-induced Depolymerization. *J Biol Chem* 287, 35127-35138**
19. **Bosc, C., Frank, R., Denarier, E., Ronjat, M., Schweitzer, A., Wehland, J., and Job, D. (2001) Identification of novel bifunctional calmodulin-binding and microtubule-stabilizing motifs in STOP proteins. *J Biol Chem* 276, 30904-30913**
20. **Job, D., Fischer, E. H., and Margolis, R. L. (1981) Rapid disassembly of cold-stable microtubules by calmodulin. *Proc Natl Acad Sci U S A* 78, 4679-4682**
21. **Job, D., Rauch, C. T., Fischer, E. H., and Margolis, R. L. (1982) Recycling of cold-stable microtubules: evidence that cold stability is due to substoichiometric polymer blocks. *Biochemistry* 21, 509-515**
22. **Bouvier, D., Vanhaverbeke, C., Simorre, J. P., Arlaud, G. J., Bally, I., Forge, V., Margolis, R. L., Gans, P., and Kleman, J. P. (2003) Unusual Ca(2+)-calmodulin binding interactions of the microtubule-associated protein F-STOP. *Biochemistry* 42, 11484-11493**
23. **Castoldi, M., and Popov, A. V. (2003) Purification of brain tubulin through two cycles of polymerization-depolymerization in a high-molarity buffer. *Protein Expr Purif* 32, 83-88**
24. **Chernov, K. G., Curmi, P. A., Hamon, L., Mechulam, A., Ovchinnikov, L. P., and Pastre, D. (2008) Atomic force microscopy reveals binding of mRNA to microtubules mediated by two major mRNP proteins YB-1 and PABP. *FEBS Lett* 582, 2875-2881**
25. **Grzesiek, S., and Bax, A. (1993) Amino acid type determination in the sequential assignment procedure of uniformly 13C/15N-enriched proteins. *J Biomol NMR* 3, 185-204**
26. **Johnson, B. A., and Blevins, R. A. (1994) NMR View: A computer program for the visualization and analysis of NMR data. *J Biomol NMR* 4, 603-614**
27. **Favier, A., and Brutscher, B. (2011) Recovering lost magnetization: polarization enhancement in biomolecular NMR. *J Biomol NMR* 49, 9-15**
28. **Delaglio, F., Grzesiek, S., Vuister, G. W., Zhu, G., Pfeifer, J., and Bax, A. (1995) NMRPipe: a multidimensional spectral processing system based on UNIX pipes. *J Biomol NMR* 6, 277-293**
29. **Humphrey, W., Dalke, A., and Schulten, K. (1996) VMD: visual molecular dynamics. *J Mol Graph* 14, 33-38, 27-38**
30. **Lieuvin, A., Labbe, J. C., Doree, M., and Job, D. (1994) Intrinsic microtubule stability in interphase cells. *J Cell Biol* 124, 985-996**
31. **Chernov, K. G., Mechulam, A., Popova, N. V., Pastre, D., Nadezhdina, E. S., Skabkina, O. V., Shanina, N. A., Vasiliev, V. D., Tarrade, A., Melki, J., Joshi, V., Baconnais, S., Toma, F., Ovchinnikov, L. P., and Curmi, P. A. (2008) YB-1 promotes microtubule assembly in vitro through interaction with tubulin and microtubules. *BMC Biochem* 9, 23**
32. **Wishart, D. S., Bigam, C. G., Yao, J., Abildgaard, F., Dyson, H. J., Oldfield, E., Markley, J. L., and Sykes, B. D. (1995) 1H, 13C and 15N chemical shift referencing in biomolecular NMR. *J Biomol NMR* 6, 135-140**
33. **Lefevre, J., Chernov, K. G., Joshi, V., Delga, S., Toma, F., Pastre, D., Curmi, P. A., and Savarin, P. (2011) The C terminus of tubulin, a versatile partner for cationic molecules: binding of Tau, polyamines, and calcium. *J Biol Chem* 286, 3065-3078**
34. **Ban, C., Ramakrishnan, B., Ling, K. Y., Kung, C., and Sundaralingam, M. (1994) Structure of the recombinant Paramecium tetraurelia calmodulin at 1.68 A resolution. *Acta Crystallogr D Biol Crystallogr* 50, 50-63**
35. **Bonnet, C., Denarier, E., Bosc, C., Lazereg, S., Denoulet, P., and Larcher, J. C. (2002) Interaction of STOP with neuronal tubulin is independent of polyglutamylation. *Biochem Biophys Res Commun* 297, 787-793**

inserm-00858655, version 1 - 5 Sep 2013

36. **Al-Bassam, J., Ozer, R. S., Safer, D., Halpain, S., and Milligan, R. A. (2002) MAP2 and tau bind longitudinally along the outer ridges of microtubule protofilaments. *J Cell Biol* 157, 1187-1196**

37. **Moores, C. A., Perderiset, M., Francis, F., Chelly, J., Houdusse, A., and Milligan, R. A. (2004) Mechanism of microtubule stabilization by doublecortin. *Mol Cell* 14, 833-839**

38. **Makarov, A. A., Tsvetkov, P. O., Villard, C., Esquieu, D., Pourroy, B., Fahy, J., Braguer, D., Peyrot, V., and Lafitte, D. (2007) Vinflunine, a novel microtubule inhibitor, suppresses calmodulin interaction with the microtubule-associated protein STOP. *Biochemistry* 46, 14899-14906**

39. **Kakiuchi, S., and Sobue, K. (1981) Ca2+-and calmodulin-dependent flip-flop mechanism in microtubule assembly-disassembly. *FEBS Lett* 132, 141-143**

40. **Baratier, J., Peris, L., Brocard, J., Gory-Faure, S., Dufour, F., Bosc, C., Fourest-Lieuvin, A., Blanchoin, L., Salin, P., Job, D., and Andrieux, A. (2006) Phosphorylation of microtubule-associated protein STOP by calmodulin kinase II. *J Biol Chem* 281, 19561-19569**

41. **He, L., Hou, Z., and Qi, R. Z. (2008) Calmodulin binding and Cdk5 phosphorylation of p35 regulate its effect on microtubules. *J Biol Chem* 283, 13252-13260**

42. **Lee, Y. C., and Wolff, J. (1984) The calmodulin-binding domain on microtubule-associated protein 2. *J Biol Chem* 259, 8041-8044**

43. **Kotani, S., Nishida, E., Kumagai, H., and Sakai, H. (1985) Calmodulin inhibits interaction of actin with MAP2 and Tau, two major microtubule-associated proteins. *J Biol Chem* 260, 10779-10783**

44. **Padilla, R., Maccioni, R. B., and Avila, J. (1990) Calmodulin binds to a tubulin binding site of the microtubule-associated protein tau. *Mol Cell Biochem* 97, 35-41**

45. **Meador, W. E., Means, A. R., and Quiocho, F. A. (1993) Modulation of calmodulin plasticity in molecular recognition on the basis of x-ray structures. *Science* 262, 1718-1721**

46. **Osawa, M., Tokumitsu, H., Swindells, M. B., Kurihara, H., Orita, M., Shibanuma, T., Furuya, T., and Ikura, M. (1999) A novel target recognition revealed by calmodulin in complex with Ca2+-calmodulin-dependent kinase kinase. *Nat Struct Biol* 6, 819-824**

47. **McIlroy, B. K., Walters, J. D., Blackshear, P. J., and Johnson, J. D. (1991) Phosphorylation-dependent binding of a synthetic MARCKS peptide to calmodulin. *J Biol Chem* 266, 4959-4964**

48. **Blackshear, P. J. (1993) The MARCKS family of cellular protein kinase C substrates. *J Biol Chem* 268, 1501-1504**

49. **Minami, Y., Kawasaki, H., Suzuki, K., and Yahara, I. (1993) The calmodulin-binding domain of the mouse 90-kDa heat shock protein. *J Biol Chem* 268, 9604-9610**

50. **Larkin, M. A., Blackshields, G., Brown, N. P., Chenna, R., McGettigan, P. A., McWilliam, H., Valentin, F., Wallace, I. M., Wilm, A., Lopez, R., Thompson, J. D., Gibson, T. J., and Higgins, D. G. (2007) Clustal W and Clustal X version 2.0. *Bioinformatics* 23, 2947-2948**

51. **Livingstone, C. D., and Barton, G. J. (1993) Protein sequence alignments: a strategy for the hierarchical analysis of residue conservation. *Comput Appl Biosci* 9, 745-756**

52. **Mulder, F. A., Schipper, D., Bott, R., and Boelens, R. (1999) Altered flexibility in the substrate-binding site of related native and engineered high-alkaline Bacillus subtilisins. *J Mol Biol* 292, 111-123**

Acknowledgments- We thank Rabia Letaief for her help for NMR resonances assignment and Imane Hamdi for cell culture experiments. We thank Sylviane Hoos and Patrick England from la Plate-forme de biophysique des macromolécules et de leurs interactions (Institut Pasteur, Paris, France) for help, technical support and fruitful discussions.

inserm-00858655, version 1 - 5 Sep 2013

inserm-00858655, version 1 - 5 Sep 2013

FOOTNOTES

*****Recipient of a postdoctoral fellowship from the PRES UniversSud

The abbreviations used are: AFM, atomic force microscopy; BSA, bovine serum albumin; CaM, calmodulin; CaMKII, Ca^{2+}-Calmodulin-dependent protein kinase II; DMEM, Dulbecco's modified Eagle medium; DTT, dithiothreitol; EGTA, ethylene glycol tetraacetic acid; GTP, guanosine 5'-triphosphate; MAP, microtubules-associated protein; ITC, isothermal titration calorimetry; NMR, nuclear magnetic resonance; MT(s), microtubule(s); SDS-PAGE, sodium dodecyl sulfate polyacrylamide gel electrophoresis; STOP, stable tubule only polypeptide

FIGURE LEGENDS

FIGURE 1. Mn modules from MAP6-N are conserved across species. A. Schematic representation of the MAP6-N protein (Rattus norvegicus). B. Sequence alignment of MAP6-N Mn1 and Mn2 modules from different species obtained with the ClustalW2 software (50). Conservation is based on the AMAS method of multiple sequence alignment analysis and reflects the conservation of physico-chemical properties of amino acids (51). Accession numbers are: Rn *NP_058900* (NCBI), Mum *NP_001041632* (NCBI), Hs *AAI50255* (GenBank), Mam *AFJ70456* (GenBank), Dc *XP_534007* (NCBI), Ss *NP_001167398* (NCBI), Tn *CAF90592* (GenBank), Gg *NP_990250* (NCBI), Xt *NP_001120222* (NCBI). C. Sequence alignment of the three Mn modules of MAP6-N (Rattus norvegicus).

FIGURE 2. $MAP6_{90\text{-}177}$ induces MT resistance to cold and nocodazole in HeLa cells. HeLa cells were transfected with the pCMV-FLAG- $MAP6_{90\text{-}177}$ plasmid. 48 h after transfection, cells were either exposed to ice or to 20 μM nocadazole for 30 min, fixed/permeabilized and then stained with anti-tubulin and anti-FLAG antibodies (bar = 5 μm).

FIGURE 3. $MAP6_{90\text{-}177}$ binds in vitro to MTs and induces MT resistance to the cold. A. SDS-PAGE analysis of MT co-sedimentation assay. Increasing concentrations of taxol-stabilized MTs were incubated with a fixed amount of $MAP6_{90\text{-}177}$ (20 μM) and centrifuged. The pellet fractions containing MTs and co-sedimented $MAP6_{90\text{-}177}$ were run on SDS-PAGE and revealed by Coomassie blue staining. B. Saturation curve of $MAP6_{90\text{-}177}$ fixation to MTs. $MAP6_{90\text{-}177}$ at different concentration was incubated with a fixed amount of taxol-stabilized MTs (10 μM). MT-bound $MAP6_{90\text{-}177}$ was quantified by SDS-PAGE using an Odyssey Imaging System. Error bars are from three independent experiments. C. SDS-PAGE analysis of MT stabilization assay. 25 μM tubulin was polymerized at 37°C for 30 min without or with 20 μM $MAP6_{90\text{-}177}$. After incubation on ice (or 37°C for the control) for 10 min, MT pellets were collected by centrifugation at 4°C (or 37°C for the control) and analyzed by SDS-PAGE and Coomassie blue staining. D. MT formation was assessed by turbidimetry. 35 μM tubulin was polymerized with varying concentrations of $MAP6_{90\text{-}177}$ at 37°C: 0 (full line), 0.35 (thick dashed line), 3.5 (thin dashed line) and 35 μM (dot line). MT destabilization was induced by a cold shock at t = 23 min (2 min at 4°C) and temperature was then set again at 37°C. E. AFM imaging. Image was recorded at t = 30 min in the presence of 35 μM $MAP6_{90\text{-}177}$ (bar = 1 μm).

FIGURE 4. $MAP6_{90\text{-}177}$ interacts with Ca^{2+}-CaM (K_d = 0.4 μM). A. $MAP6_{90\text{-}177}$ binds only to the holoform of CaM. $MAP6_{90\text{-}177}$ was incubated with CaM-agarose beads in the presence or absence of Ca^{2+}. Beads were then washed and flow-through, washes and CaM-beads fractions were analyzed on SDS-PAGE and revealed by Coomassie blue staining. B. ITC analysis of the interaction of $MAP6_{90\text{-}177}$ with Ca^{2+}-CaM. Heat signal is shown (top) with the binding isotherm derived from this signal (bottom). C. Parameters obtained from the best fit.

FIGURE 5. Structural analysis of $MAP6_{90\text{-}177}$. A. Assigned $MAP6_{90\text{-}177}$ ^{1}H-^{15}N HSQC spectrum in 50 mM MES-KOH, 150 mM NaCl, 1mM DTT, pH 6.9 at 20°C. Some indeterminations remained for

residues marked with triangles (E151 or R166), stars (K156) and rectangles (Q142, E149 or Q155). B. Corresponding secondary chemical shifts for ^{13}CO and $^{13}C\alpha$ illustrating the absence of secondary structure.

FIGURE 6. MTs and Ca^{2+}-CaM compete for the same binding site on $MAP6_{90-177}$. A. NMR analysis of $MAP6_{90-177}$:MT and $MAP6_{90-177}$:Ca^{2+}-CaM interactions. ^{1}H-^{15}N HSQC spectra of ^{15}N-labeled $MAP6_{90-177}$:MT (molar ratio 1:2, 6°C) and ^{15}N-labeled $MAP6_{90-177}$:Ca^{2+}-CaM (molar ratio 1:3, 20°C) complexes. The $MAP6_{90-177}$ residues implicated in the binding of MTs and Ca^{2+}-CaM are highlighted in bold (proline residues lying in or around the sequences were arbitrarily included). B. Ca^{2+}-CaM competes with MTs for $MAP6_{90-177}$ binding. 35 µM taxol-stabilized MTs were incubated with 10 µM $MAP6_{90-177}$, 0.2 mM $CaCl_2$ and varying concentrations of CaM for 5 min at 20°C. After centrifugation, pellet and supernatant contents were analyzed by SDS-PAGE and Coomassie blue staining. Stars correspond to experiments where 0.2 mM $CaCl_2$ was replaced by 0.5 mM EGTA. C. Ca^{2+}-CaM inhibits the protective effect of $MAP6_{90-177}$ on MTs. 35 µM tubulin was polymerized in the presence of 0.5 mM spermine to counteract the negative effects of Ca^{2+} on MTs. After addition of 50 µM $CaCl_2$, polymerized MTs were incubated on ice for 10 min alone (control, the two left lanes) or with 25 µM $MAP6_{90-177}$ (the two middle lanes) and 100 µM CaM (the two right lanes). Pellets and supernatants contents were analyzed by SDS-PAGE and Coomassie blue staining.

FIGURE 7. Ca^{2+}-CaM undergoes large conformational changes when in interaction with $MAP6_{90-177}$. A. BEST-TROSY spectra superposition of ^{15}N-^{13}C-labeled Ca^{2+}-CaM in the absence (red) and presence of $MAP6_{90-177}$ (0.5:1 $MAP6_{90-177}$:Ca^{2+}-CaM molar ratio) (gray). Residues that are not significantly affected by the interaction (no line broadening nor significant chemical shift perturbation $(((\Delta\delta^{1}H)^2 + (\Delta\delta^{15}N/6.5)^2)^{1/2} < 0.09$ ppm, (52)) are labeled. B. Sequence of CaM showing the residues affected by the interaction (bold). The proline P67 residue was arbitrarily included. The central α helix separating the N- and C-terminal domains of CaM is underlined. C. Spatial representations of the Ca^{2+}-CaM structure (PDB code: 1OSA). Figure on the right was obtained after a 180° rotation around the x axis and a 90° rotation around the z axis. Residues which are not significantly affected by the interaction are rendered as gray rigid blocks. Yellow balls: Ca^{2+} ions.

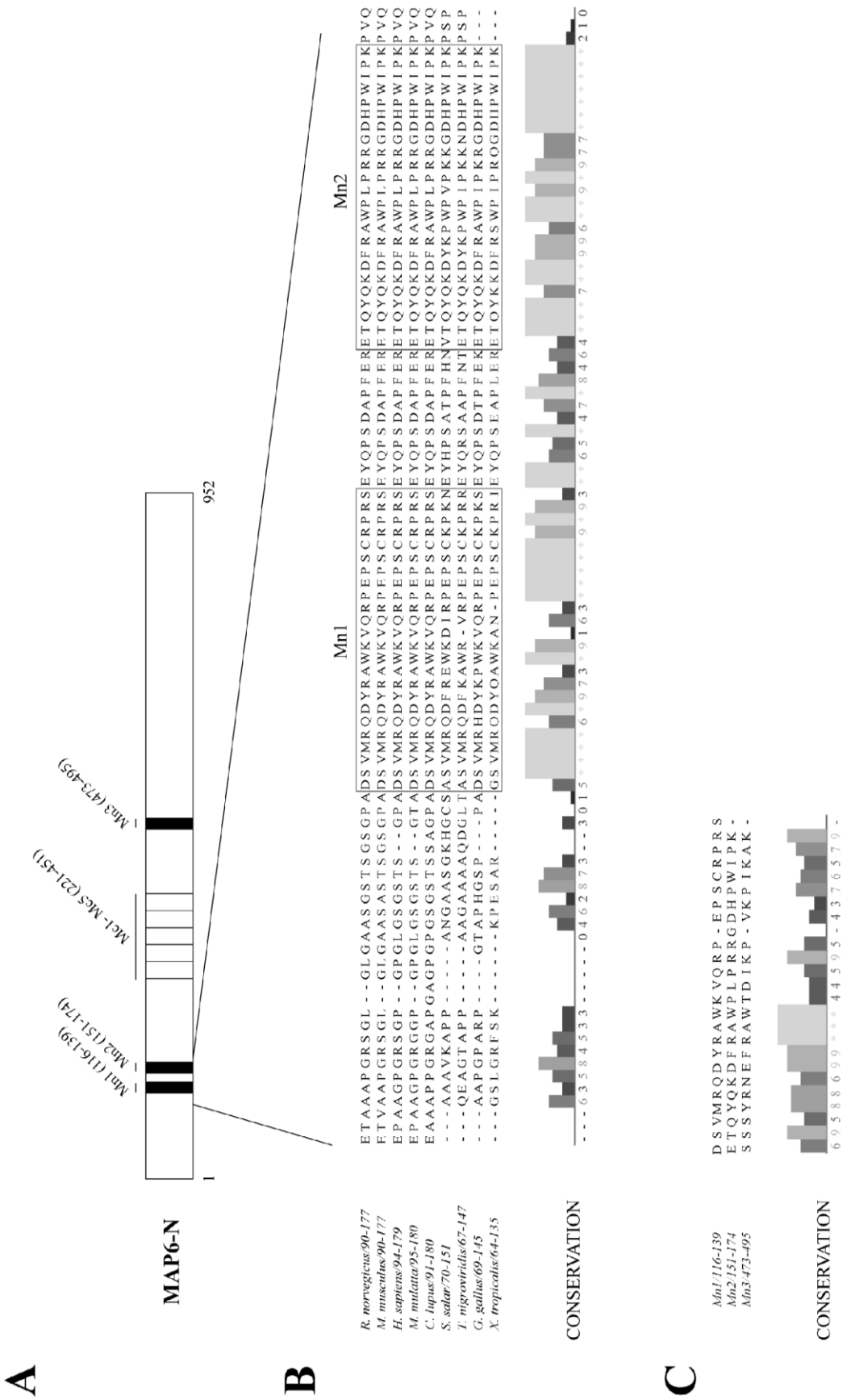
FIGURE 8. The Mn1 module of MAP6-N (residues 90-142, $MAP6_{90-142}$) interacts with MTs and Ca^{2+}-CaM. A. NMR analysis of $MAP6_{90-142}$:MT and $MAP6_{90-142}$:Ca^{2+}-CaM interactions. ^{1}H-^{15}N HSQC spectra of ^{15}N-labeled $MAP6_{90-142}$:MT and ^{15}N-labeled $MAP6_{90-142}$:Ca^{2+}-CaM complexes (1:1 molar ratio at 6°C and 1:3 molar ratio at 20°C respectively). B. Residues implicated in the binding of MTs and Ca^{2+}-CaM are highlighted in bold in the $MAP6_{90-142}$ sequence (proline residues lying in the sequences were arbitrarily included).

FIGURE 9. CaM 1-5-10 binding motif alignment. Sequence alignment of 1-5-10 class motifs from selected CaM-binding partners. The Ca^{2+}-CaM interacting region delimited by NMR $MAP6_{90-177}$ comprises two canonical CaM binding motifs belonging to the 1-5-10 class.

FIGURES

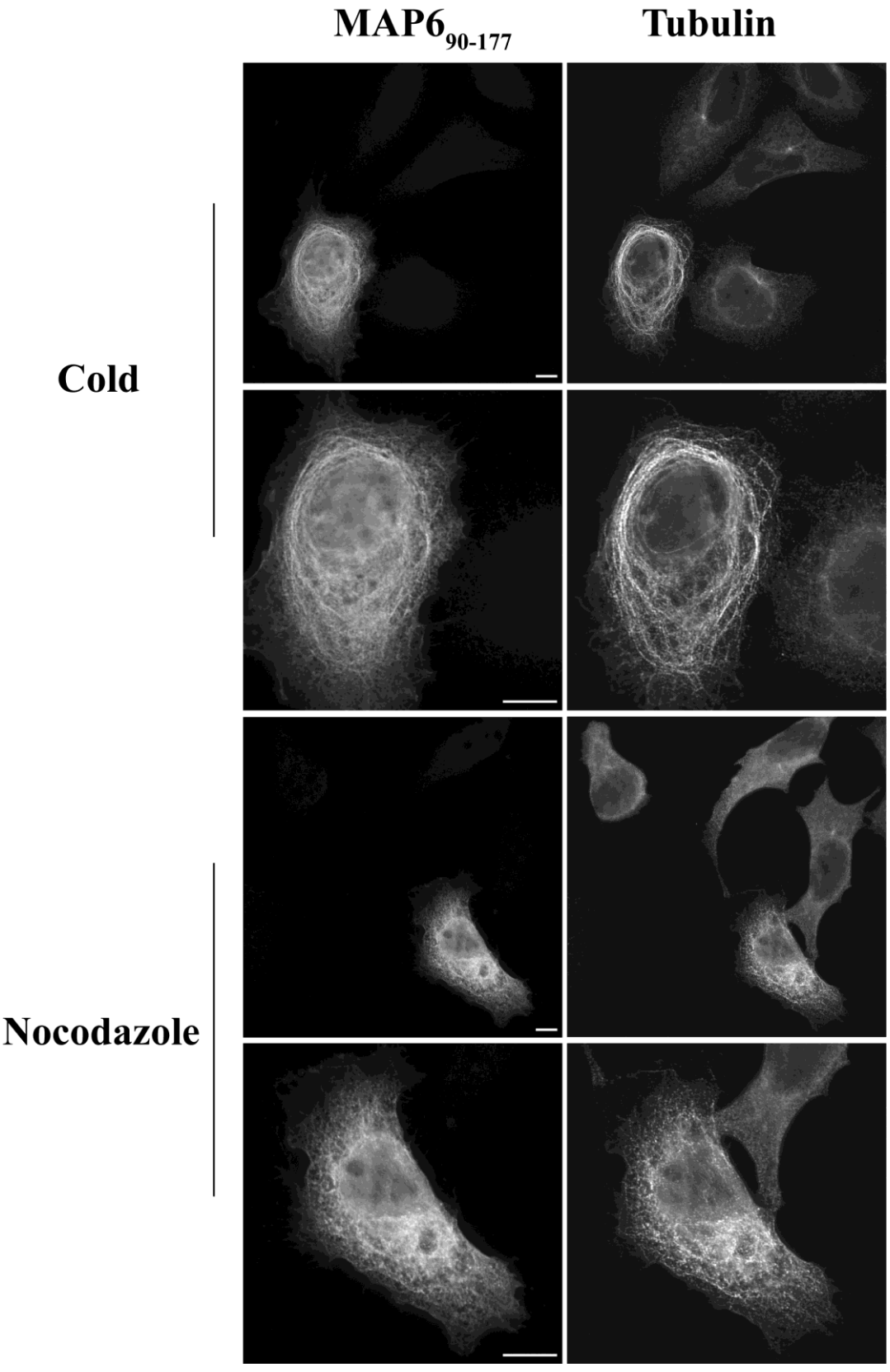
inserm-00858655, version 1 - 5 Sep 2013

Figure 1



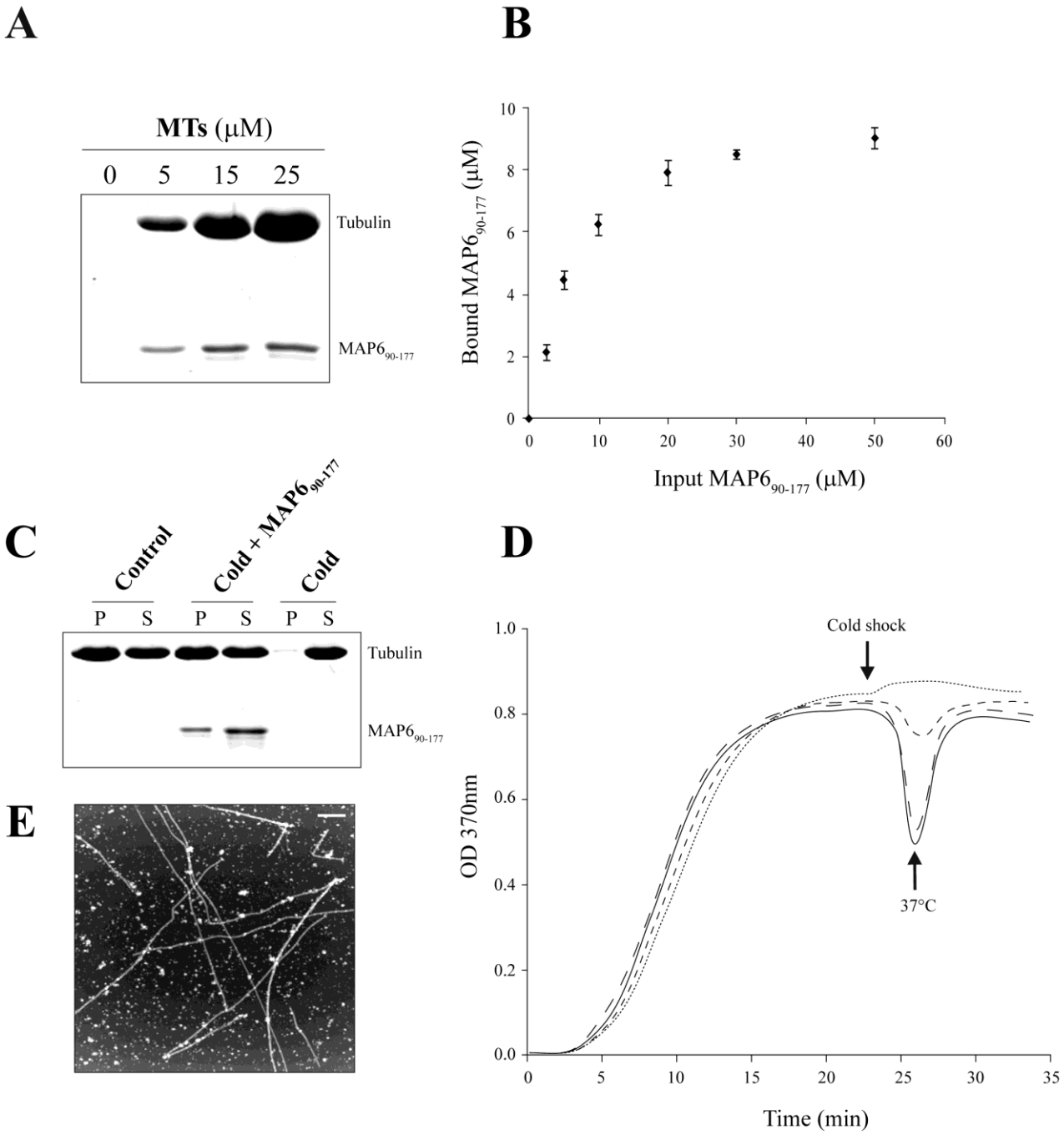
inserm-00858655, version 1 - 5 Sep 2013

Figure 2



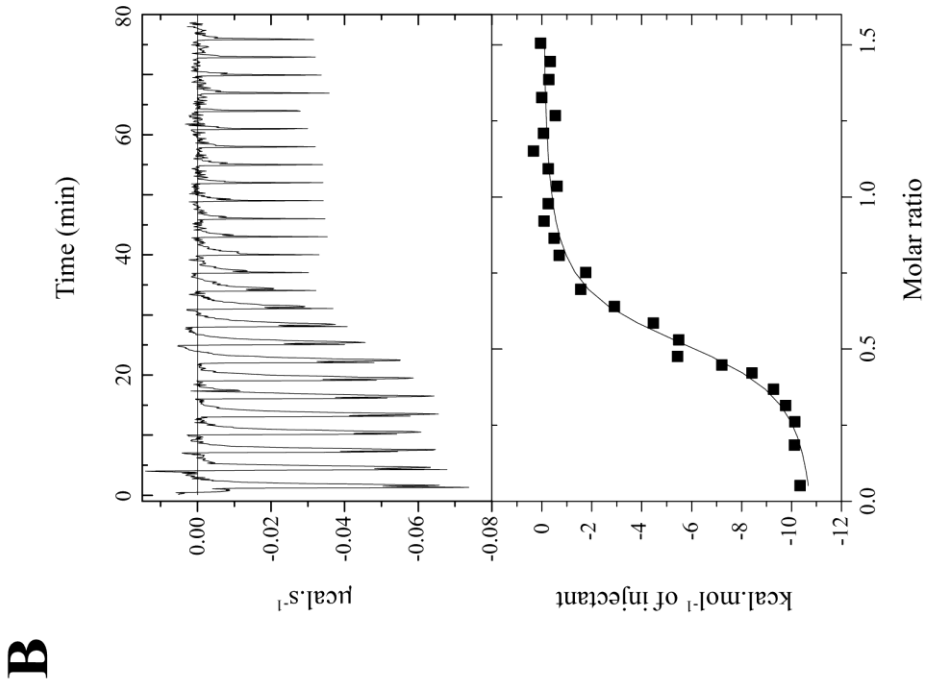
inserm-00858655, version 1 - 5 Sep 2013

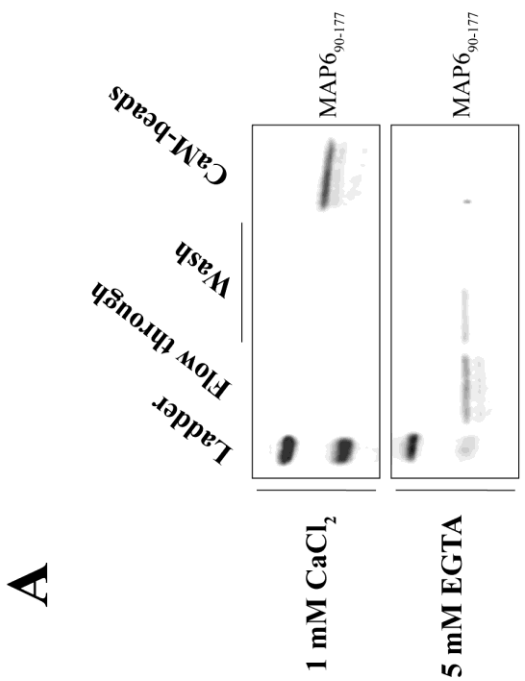
Figure 3



inserm-00858655, version 1 - 5 Sep 2013

Figure 4



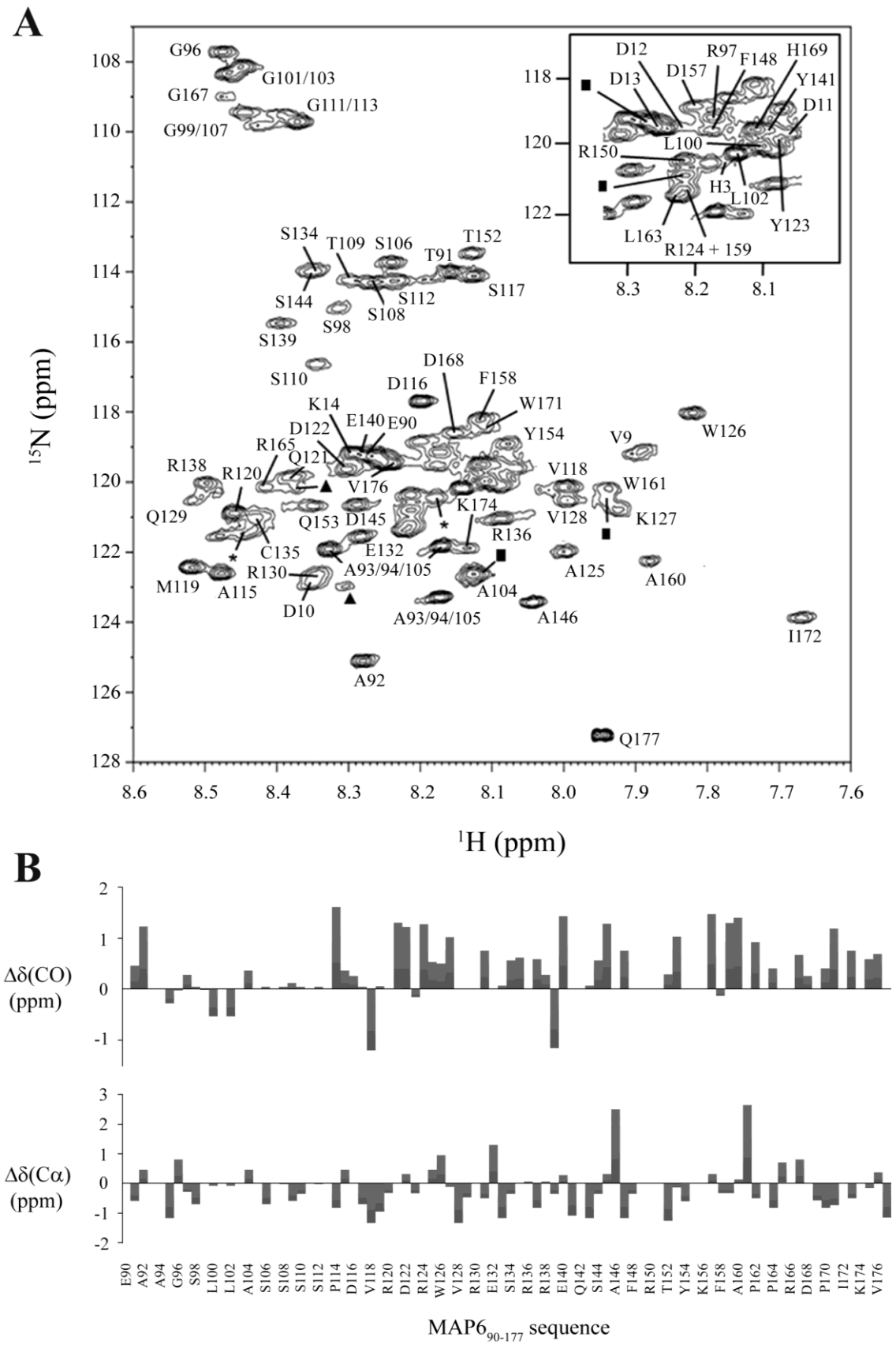


C

Stoichiometry	0.515 +/- 0.01
Kd (mol.L^{-1})	4.40 x 10^{-7} +/- 8.69 x 10^{-8}
ΔH (kcal.mol^{-1})	- 11.08 +/- 0.379
ΔS (cal.mol^{-1}.K^{-1})	- 8.71

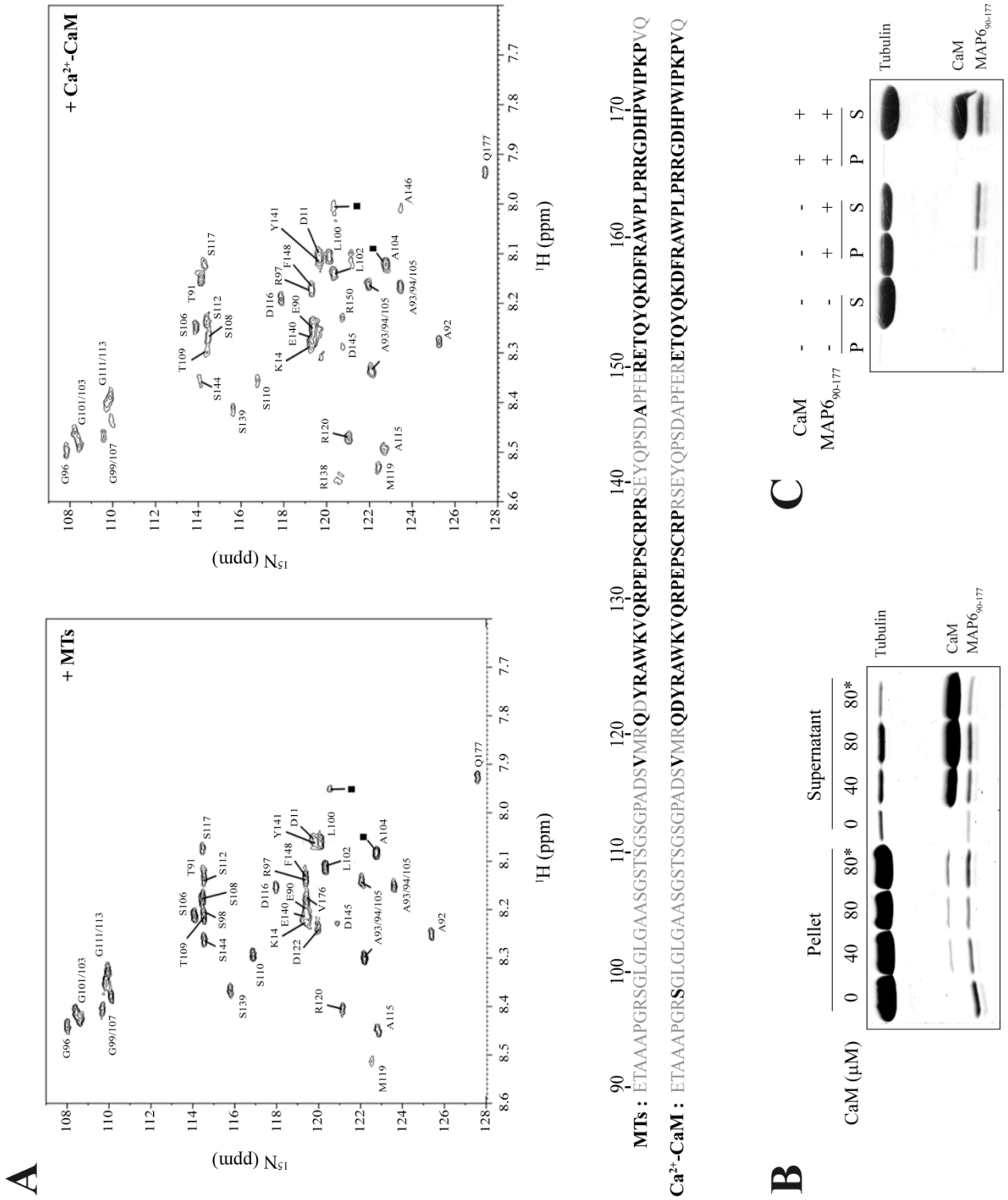
inserm-00858655, version 1 - 5 Sep 2013

Figure 5



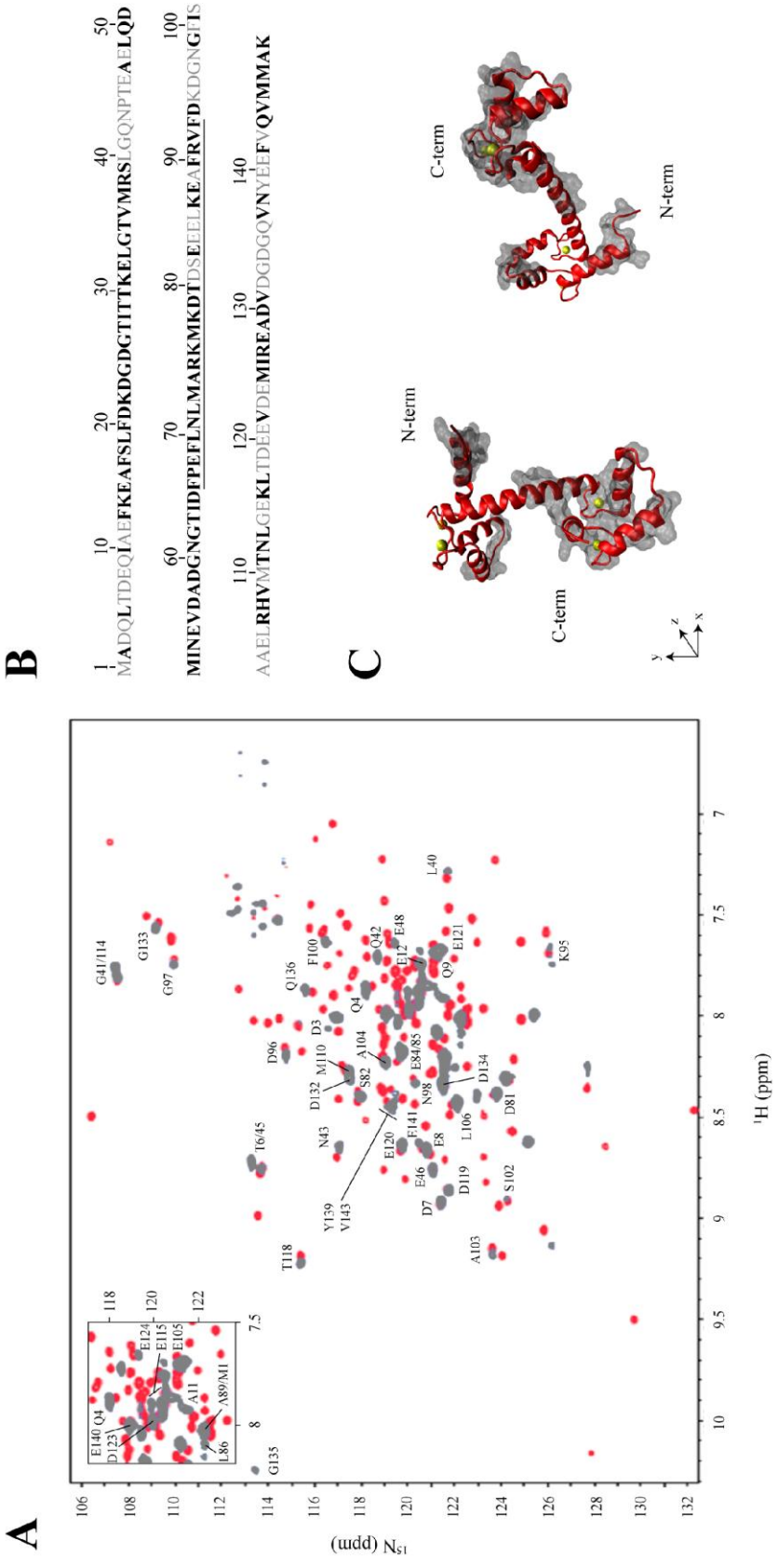
inserm-00858655, version 1 - 5 Sep 2013

Figure 6



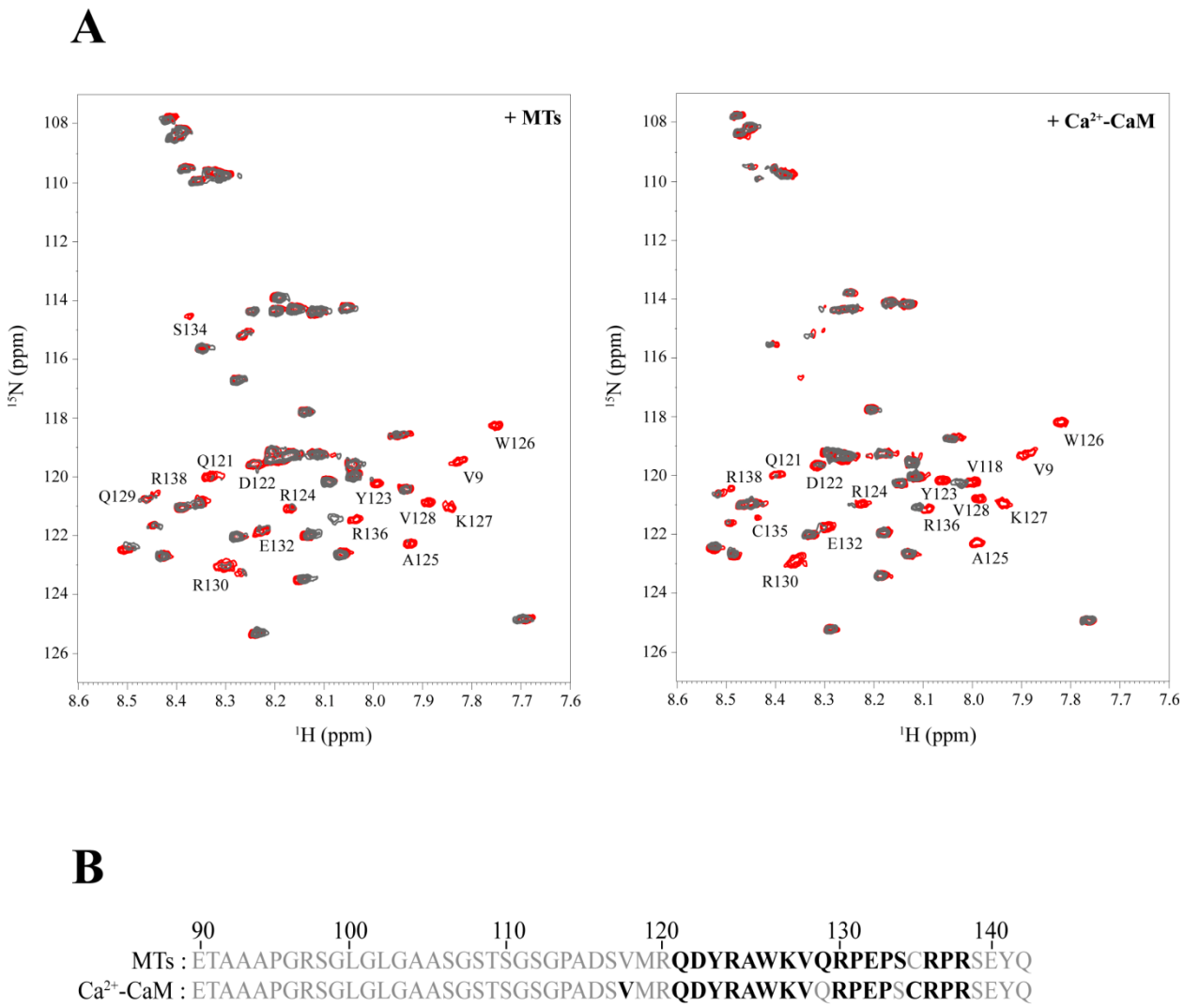
inserm-00858655, version 1 - 5 Sep 2013

Figure 7



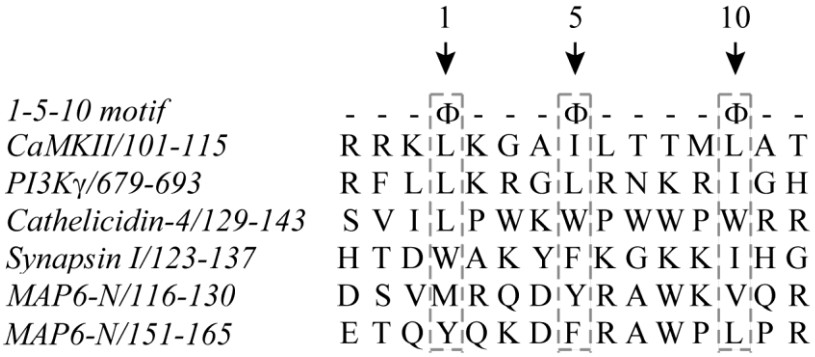
inserm-00858655, version 1 - 5 Sep 2013

Figure 8



inserm-00858655, version 1 - 5 Sep 2013

Figure 9



inserm-00858655, version 1 - 5 Sep 2013